# The I*($^2P_{1/2}$)−I*($^2P_{1/2}$) Contact Pair Emission in Condensed Media: A Molecular Spring-Gauge for Cavity Sizing†

**M. Karavitis and V. A. Apkarian***

*Department of Chemistry, UC Irvine, California 92697*

*Received: April 25, 2002; In Final Form: June 6, 2002*

The I*I*($0_g^+$) → I*I(B($0_u^+$)) emission spectra obtained in neat Ar, Kr, Xe, and in mixed Kr/Xe matrixes is reported. The emission from the strictly cage-bound initial state shifts linearly with Kr/Xe mixing fraction, without significant change in spectral width. The line shapes in mixed-hosts are understood in terms of the statistics of sites in the solid solutions. The pure-host line shapes are reproduced through Monte Carlo simulations using accurately known I−Rg potentials. The analysis yields a refined I*I* potential and provides a calibration curve to readout the cavity size of isolation from the observed emission peak shift.

## Introduction

The interaction between spin-excited iodine atoms, I*($^2P_{1/2}$) + I*($^2P_{1/2}$), leads to three potentials, $0_g^+$, $0_g^-$, and $1_u$, all three of which are repulsive (see Figure 1).[2] At contact, the spin-flip transitions to I*($^2P_{1/2}$) + I($^2P_{3/2}$) and I($^2P_{1/2}$) + I($^2P_{1/2}$) are dipole-allowed through Hund's case (c) selection rules, $\Delta\Omega = 0, \pm 1$. We have previously reported on these spin-flip transitions in a variety of liquids at room temperature and in the cryogenic rare gas matrixes of Ar, Kr, and Xe.[2] We recognize that these condensed phase emission spectra are of interest as reporters of local structure, because the contact distance in the emitting state is strictly determined by the solvent cage. Among the allowed transitions, the I*I*($0_g^+$) → I*I(B($0_u^+$)) fluorescence which terminates on the attractive wall of the deeply bound B state is particularly useful, because it undergoes a large spectral shift as a function of the internuclear distance in the emitting state. Accordingly, the spectral shift of this transition should provide a direct readout of the size of the cavity in which the molecule resides, hence, the title analogy of a spring-gauge.

We present spectra obtained in mixed Kr/Xe matrixes to illustrate the suggested application in heterogeneous media. The spectra are analyzed through detailed simulations, to understand their dependence on the nature of the host and to provide a quantitative calibration of the gauge. It is hoped that this tool will find practical use in materials characterization. Iodine can be introduced as a dopant in a great variety of solid-state materials, from photovoltaic solids,[3] to photoconductive polymers,[4,5] zeolites,[6] to clatharates.[7] These are also examples of systems for which information about local structure is valuable. With the motivation of characterizing the local cage, time-resolved studies of iodine have already been carried out in nanocavities in porous silica[8,9] and in cyclodextrene.[10] An additional motivation of the mixed solids is to investigate the effect of local cage symmetry on dynamics and in particular on the electronic caging process which had been suggested based on the contrast of predissociation of $I_2$(B) in liquid and solid phases.[11]

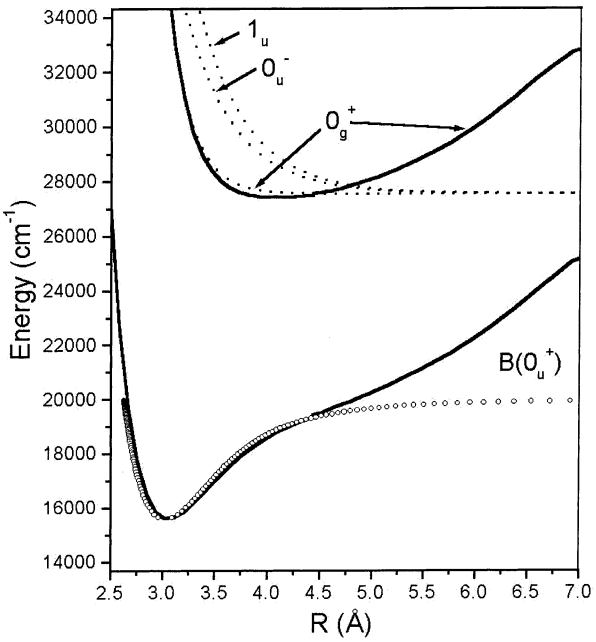


**Figure 1.** Relevant potential energy curves of iodine. The solid curves represent the solvated potentials, calculated by relaxing the lattice for a given I*−I*($0_g^+$) distance. The gas-phase curves are also indicated. The B($O_u^+$) potential (open circles) is the RKR parametrization of ref 24. The three I*($^2P_{1/2}$) + I*($^2P_{1/2}$) states of molecular iodine are shown as dotted lines.

## Experimental Section

Starting with molecular iodine in its ground electronic state, the I*I* potentials can be accessed through a variety of optical pumping schemes. Resonant two-photon excitation with the B($^3\Pi_{0u}$) state acting as intermediate is useful when using short pulses.[2] Two-photon resonant excitation with long-lived intermediate states can be induced with cw lasers.[12] In polar solvents, these states can be most efficiently reached indirectly, via the predissociation of the ion-pair states.[11,13] The latter can be accessed either through one-photon UV pumping or two-photon excitation in the visible by taking advantage of the strong transition dipoles associated with the ion-pair states.[14,15] The

† Part of the special issue "John C. Tully Festschrift".

* To whom correspondence should be addressed. E-mail: aapkaria@uci.edu.

10.1021/jp0260191 CCC: $22.00 
Published on Web 07/02/2002

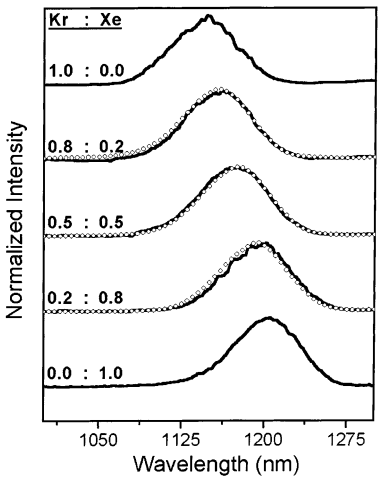


**Figure 2.** Plot of the I*I*($0_g^+$) → I*I(B($0_u^+$)) emission spectra for $I_2$ in krypton, xenon, and in Kr/Xe solutions: Experiment (solid curve) and theory according to eq 2 of text (open circles). The spectral shift of these emissions varies linearly with the mixing fraction, while the widths remain constant.

**TABLE 1: Spectral Parameters for the I*I*($0_g^+$) → I*I-(B($0_u^+$)) Emission in Pure Kr, Xe, and Mixed Kr/Xe Matrixes**

| mixing fraction Kr:Xe | $\lambda_{peak}$ (nm) | $\Delta\lambda_{fwhm}$ (nm) |
|---|---|---|
| 1.0:0.0 | 1145.0 | 69.0 |
| 0.8:0.2 | 1157.6 | 70.6 |
| 0.5:0.5 | 1171.4 | 73.2 |
| 0.2:0.8 | 1194.2 | 68.9 |
| 0.0:1.0 | 1201.7 | 70.2 |

present spectra were obtained while conducting time-resolved pump−probe measurements on the B state, using 80 fs pulses near 550 nm. The near-infrared fluorescence was collected through a $^1/_4$ m scanning monochromator (Schoefel, Inc.) and detected using a liquid nitrogen cooled Ge detector (ADC, model 403H). The output from the detector was boxcar averaged (SRS), digitized, and recorded on a personal computer.

The cryogenic matrixes were prepared by continuously depositing a premixed sample of $I_2$:Rg (1:5000) on a sapphire substrate kept at 12 K using a closed cycle helium cryostat. The gas flow was regulated using a leak valve, with the backing pressure maintained at 1000 Torr during the deposition. The thin films were allowed to grow until the sample appeared purple to the eye. Research grade gases with the manufacturer's stated purity of 99.995% (Matheson Gas Co.) were used without further purification. Iodine of 99.99+ purity (Aldrich Chemical Co.) was further purified using three freeze−pump−thaw cycles to remove trapped gases.

## Results

The I*I*($0_g$) → I*I(B($0_u$)) spectra in pure matrixes have previously been reported.[2] The emission spectra in Kr, in Xe, and in mixed Kr/Xe matrixes are shown in Figure 2. The spectral parameters, peak wavelength and full width at half-maximum (fwhm) are collected in Table 1. The observed peak wavelength is a linear function of the mixing fraction, as illustrated in Figure 3. The spectral widths are nearly independent of composition.

## Discussion

**A. Empirical Analysis of the Spectra in Kr/Xe Solid Solutions.** The empirical observation of linear dependence of the emission peak wavelength with mixing fraction, empirically, implies an ideal dependence:

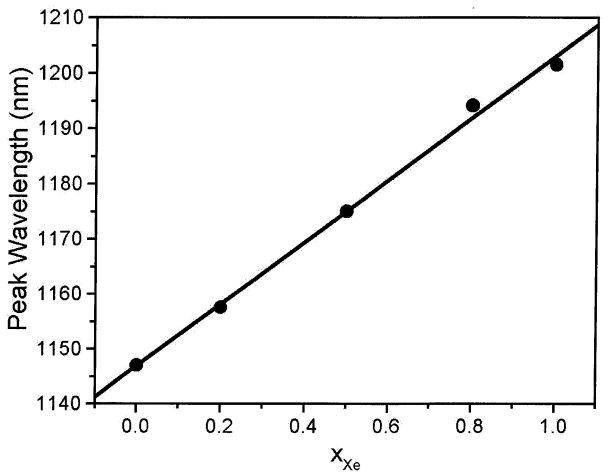


**Figure 3.** Plot of the emission peak wavelength vs mole fraction of Xe.

$$\bar{\lambda}(x_i) = \bar{\lambda}(x_i = 0) + x_i[\bar{\lambda}(x_i = 1) - \bar{\lambda}(x_i = 0)] \quad \text{where } i = \text{Kr, Xe} \quad (1a)$$

or more compactly

$$\bar{\lambda}(x_i) = \bar{\lambda}_j + x_i[\bar{\lambda}_i - \bar{\lambda}_j] \text{ where } \bar{\lambda}_j \equiv \bar{\lambda}(x_i = 0) \text{ and } \bar{\lambda}_i \equiv \bar{\lambda}(x_i = 1) \quad (1b)$$

in which the overbar indicates the peak wavelength (obtained by fitting the spectra to Gaussians). Evidently, the spectral shift is the result of the mean-field felt by iodine from the surrounding cage atoms. The independence of the spectral width on mixing ratio of the sample is noteworthy. In a given site, we expect a broad spectrum, $I(\lambda - \bar{\lambda})$, given mainly by the reflection of the thermal distribution of I*−I* interatomic distances from the attractive wall of the $I_2$(B) potential. This is supported by the observation that the spectral widths in neat Kr and neat Xe, of fwhm ∼70 nm, are nearly identical. Because the interaction between I−Rg is short range in nature, we may expect the spectral shift to be determined by the mixing fraction of the cage atoms, of which there are $N = 18$ for a divacancy site in which iodine is known to isolate.[16] Then the spectrum in the mixed host will be given as:

$$I(\lambda, x_i) = \sum_{n=0}^{N} P(n; N, x_i) I(\lambda - \bar{\lambda}(x_i)) \quad (2a)$$

where

$$P(n; x_i, N) = \frac{N!}{n!(N-n)!} x_i^n (1 - x_i)^{N-n} \quad (2b)$$

is the binomial distribution. The treatment assumes that the neighbors are indistinguishable, even though the nearest neighbors in the divacancy occur in four distinct classes according to the angle they span relative to the molecular axis.[17] In effect, the angular anisotropy of interaction between the molecule and its nearest neighbors is ignored. The continuous curves in Figure 2 were obtained using this treatment, with the experimental spectral profiles in the neat matrixes defining the pure host line shape $I(\lambda - \bar{\lambda})$. The reproduction is quite satisfactory.

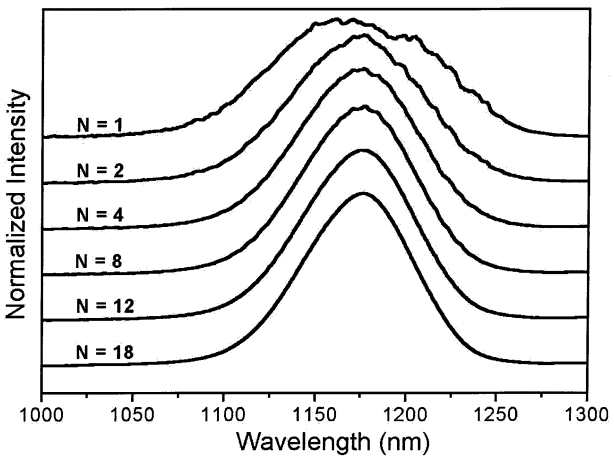


**Figure 4.** Simulated spectra of $I_2$ in a 50/50 Kr/Xe matrix for different numbers of nearest neighbors ($N$) in eq 2. $N = 18$ corresponds to isolation in a divacancy, $N = 12$ corresponds to isolation in a single substitutional site, and $N = 1$ corresponds to complete phase segregation between Kr and Xe.

The independence of the line width on mixing fraction can be understood through this model by noting that the distribution function defined by

$$D(\lambda, x_i) = \sum_{n=0}^{N} P(n; N, x_i)\delta(\lambda - \bar{\lambda}(x_i)) \tag{3}$$

is much sharper than the line shape in the pure host. For $N = 18$, the fwhm of the distribution (3) is 16 nm to be compared with the width of 70 nm in the pure host. Note that even if the molecule was isolated in a single substitutional site, for which $N = 12$, the line width in the mixed matrixes would be 72 nm, nearly identical to that in the neat solid. In Figure 4, we give the spectral shapes according to (2a) for $N = 1$ and 18. For large $N$, the spectral width can be obtained analytically. Thus, for $N > 10$, the binomial distribution is well approximated by the Gaussian

$$P(n; x_i, N) \approx \frac{1}{\sqrt{2\pi N x_i x_j}} \exp\left[-\frac{(n - Nx_i)}{2Nx_i x_j}\right] \tag{4}$$

from which the fwhm of the distribution function (3) can be obtained:

$$\text{fwhm}(D) = 2\,\frac{|\lambda_i - \lambda_j|}{N}\sqrt{Nx_i x_j 2\ln(2)} \tag{5}$$

Because the spectrum (2a) is given by the convolution of the distribution function (3) and the pure-host line shape, the overall width of the spectrum in the mixed matrixes is simply given by the geometric sum of the two widths. A noticeable broadening of the spectral line occurs for $N < 4$, which is unphysical in this model. The limit $N = 1$, namely, the simple sum of the spectra in Kr and Xe, can be identified with the case of complete segregation between the Kr and Xe matrixes, whereas $N = 2$ approximates the case of segregation into small grains, with a grain size that yields a comparable number of atoms on the surface and the bulk of the grain. Thus, the analysis clearly establishes that the mixed matrixes consist of homogeneous solid solutions, which is to be expected for equilibrium mixtures of Kr/Xe at all mole fractions.[18]

**B. Spectral Simulations: Calibration of the Gauge.** The advantage of using rare gas matrixes for establishing the connection between spectra and local structure is the simplicity and well-characterized nature of interactions, such that reliable simulations can be made. Indeed, it is the I*I* potential that is not well characterized, and the present spectra allow a determination of this potential. We carry out simulations to characterize the emission line shape in neat rare gases, to connect spectra to structure. We then verify through simulations of mixed matrixes that the spectral shifts are directly correlated to the internuclear separation between iodine atoms and insensitive to the nature of the host.

The I−Rg pair potentials have been well-characterized through scattering experiments,[19] and many-body effects on these potentials have been closely examined through spectral simulations of the I* → I transition in solid Kr and Xe[20] and zero electron kinetic energy (ZEKE) spectroscopy of the $I-Rg_n$ clusters.[21,22] The many-body contributions to these interactions are small, allowing realistic simulations under the assumption of pairwise additivity. Thus, the thermalized initial state may be simulated subject to the potential

$$V_i(R, r_i) = V_{I^*-I^*}(R) + \sum_{i=1}^{N}\sum_{j=1}^{2} V_{I^*-Rg}(|R_j - r_i|) + \frac{1}{2}\sum_{i,j} V_{Rg-Rg}(|r_i - r_j|) \tag{6a}$$

in which the I*−I* potential is assumed to be exponentially repulsive:

$$V_{I^*-I^*}(R) = A\exp(-\alpha R) \tag{6b}$$

and the angularly anisotropic I*−Rg potential is given as

$$V_{I^*-Rg}(R, \vartheta) \equiv V(II1/2) = V_0 + \frac{V_2}{10} + \frac{\Delta}{2} + \frac{1}{2}\left(\frac{9V_2^2}{25} + \Delta^2 - \frac{2V_2\Delta}{5}\right)^{1/2} \tag{6c}$$

Here, $V_0 = V_0(R)$ is the isotropic component, the anisotropic component is weighted by the second Legendre polynomial, $V_2 = V_2(R)P_2(\cos\vartheta)$, and the spin−orbit splitting is $\Delta = 7600$ $cm^{-1}$.[23] Under the assumption of the exponential form, the I*−I* potential has been constructed for the $0_g^+$ state[2] given its known energy at the $I_2(X)$ internuclear distance from absorption data and given its asymptotic limit.[1] Thus, we use this as a starting point in our simulations, to be refined by the requirement that the same potential yield the spectra in the three different solids of Ar, Kr, and Xe. The $I^*I^*(0_g^+) \rightarrow I^*I(B(0_u^+))$ emission spectrum is obtained by sampling the difference potential for thermally accessible configurations ($\{R, r_I\}$; $T$) on the I*I* surface, with the terminal state defined as

$$V_f(R, r_i) = V_{I_2(B)}(R) + \sum_{i=1}^{N}\sum_{j=1}^{2} V_{I(B)-Rg}(|R_j - r_i|) + \frac{1}{2}\sum_{i,j} V_{Rg-Rg}(|r_i - r_j|) \tag{7}$$

The $I_2(B)$ potential is well-known, and in this application, we use the accurate RKR parametrization.[24] The I−Rg interactions in the B state are also angularly anisotropic, with distance dependent $^2P_{3/2}$ and $^2P_{1/2}$ character and host-induced mixing between them.[25,26] Noting that the $I_2(B)$ wave function is the superposition $|3/2, \pm1/2\rangle|1/2, \mp1/2\rangle + |1/2, \pm1/2\rangle|3/2, \mp1/2\rangle$,

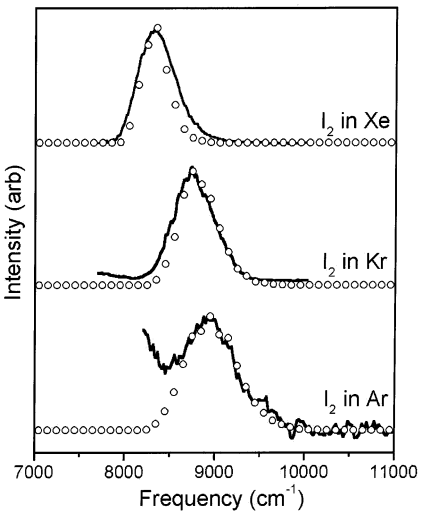


**Figure 5.** Comparison between experimental (open circles) and simulated emission spectra (solid lines) for $I_2$ in Ar, Kr, and Xe. The Monte Carlo simulation is for the constant *N*, *V*, *T* ensemble. The only adjusted parameters in this simulation are the two coefficients that define the exponentially repulsive I*−I* potential.

the I−Rg interaction in the B state can be obtained:

$$V_{I(B)-Rg}(R,\vartheta) = \frac{1}{2}(V_{X[I(^2P_{3/2})-Rg]} + V_{II[I(^2P_{1/2})-Rg]}) = V_0(R) + \frac{1}{10}V_2(R)P_2(\cos\vartheta) + \frac{\Delta}{2} \quad (8)$$

Here, $V_X$ represents the $|J = 3/2,\ \Omega = 1/2\rangle$ state and $V_{II}$ represents the $|J = 1/2,\ \Omega = 1/2\rangle$ state of I−Rg. We use Neumark's potentials for the various I−Rg pairs in eqs 6c and 8.[21,22]

The spectra are simulated using Monte Carlo methods. We consider the constant *N*, *V*, and *T* ensemble of $N = 108$ atoms, under periodic boundary conditions. We adjust *V* to minimize total energy ($P = 0$) and carry the simulations under the scaled temperature:

$$T_{sim} = \frac{\hbar\omega}{2k_B}\left[\tanh\left(\frac{\hbar\omega}{2k_B T_{exp}}\right)\right]^{-1} \quad (9)$$

in which $\omega$ is the Debye frequency of a particular solid. This correction has been demonstrated to be a useful remedy for the quantum zero-point amplitude of the lattice, which becomes significant at the cryogenic temperatures of interest.[27]

The experimental spectra in Ar, Kr, and Xe can be simultaneously reproduced, as shown in Figure 5, with the I*I* potential parametrization: $A = 6.7 \times 10^9$ cm$^{-1}$ and $\alpha = 4.51$ Å$^{-1}$. Save for the two coefficients defining this potential, there are no other adjustable parameters in the simulations.

The simulated values of the mean internuclear distance, *R***, in the initial state are collected in Table 2, along with the nearest neighbor distance in the perfect lattice. The comparison shows that the I*−I* distance in Kr and Xe is nearly identical to the nearest neighbor distances, $R_{nn}$, in the perfect lattice. Clearly, I*I* stretches to fill the divacancy cavity in which it resides. In the case of solid Ar, the I*−I* internuclear separation is ∼0.25 Å larger than $R_{nn}$, indicating that now the compressed I*I* spring is stiff enough to stretch the cavity. We may conclude that down to internuclear distances of 4 Å the spin excited molecule fills the cavity without perturbing the local cage structure. Quite generally, the internuclear distance can be read directly from the spectrum. Given the similarity of the I−Rg potentials in the initial and final state, eqs 6c and 8, the spectral shifts are determined mainly by the difference potential along the I−I coordinate. As such, the relation between spectral shift and *R*** is essentially independent of the nature of the host and can be obtained by inversion of the difference potential, $\Delta V(R) = V(I^*I^*) - V(I_2(B))$, which is shown as the dotted line in Figure 6. To expand the range of evaluation beyond the limited structures visited at thermal equilibrium; we artificially freeze the I*−I* distance at various lengths, relax the lattice, and then evaluate the spectral shifts. These points are shown in Figure 6 to closely follow the difference potential curve. The explicitly simulated points yield the calibration curve for R** versus emission peak $\bar{\omega}$, which can be fit by the analytic form

$$R^{**} = r + \frac{c}{\bar{\omega} - 7570} + \frac{1}{b}\ln\left(\frac{d}{\bar{\omega} - 7600}\right) \quad \text{for } R^{**} > 3.4 \text{ Å} \quad (10a)$$

with

$$r = 3.37 \text{ Å},\quad b = 2.51 \text{ Å}^{-1},\quad c = 136.6 \text{ cm}^{-1}\text{ Å},\quad d = 4885 \text{ cm}^{-1} \quad (10b)$$

**TABLE 2: Solvent Parameters Used in Generating Figure 6**[a]

| solvent | $R_{nn}$ (Å) | *R*** (Å) | *D* (Å) | emission peak (cm$^{-1}$) |
|---|---|---|---|---|
| $CS_2$[b] | 4.64 | 6.03 | 10.39 | 7695 |
| $CF_2Cl-CFCl_2$[b] | 5.82 | 5.52 | 9.88 | 7750 |
| $CCl_4$[b] | 5.44 | 5.36 | 9.72 | 7775 |
| $CHCl_3$[b] | 5.11 | 4.95 | 9.31 | 7880 |
| $CH_2Cl_2$[b] | 4.74 | 4.82 | 9.18 | 7930 |
| $CH_2COCH_2$[b] | 4.97 | 4.85 | 9.21 | 7920 |
| $CH_3CN$[b] | 4.50 | 4.58 | 8.93 | 8070 |
| Ar | 3.75 | 4.00 (3.98)[c] | 8.36 | 8909 |
| Kr | 4.00 | 4.07 (4.03) | 8.43 | 8730 |
| Xe | 4.33 | 4.32 (4.30) | 8.68 | 8314 |

[a] $R_{nn}$ is the nearest neighbor distance for the neat solvent, *R*** is the mean I−I distance in the I*I* State, and *D* is the cavity diameters extracted from eq 10. [b] Liquid-phase emission peaks are from ref 2 [c] In parentheses are *R*** values obtained directly from the simulations; otherwise, all values are obtained from the calibration curve of eq 10.

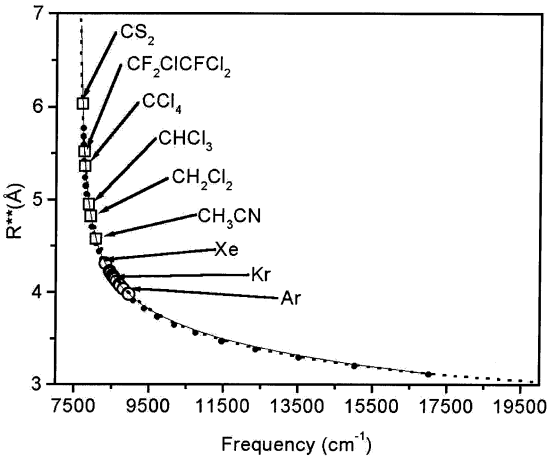


**Figure 6.** Plot of the I*I*($0_g^+$) → I*I(B($0_u^+$) emission peak versus internuclear distance, *R***. The open circles are simulations of mixed Kr/Xe solids of various composition, at thermal equilibrium ($T = $ K); the closed circles are obtained by artificially freezing the I*−I* distance and allowing the lattice to equilibrate; the dashed line is the one-dimensional difference potential between I*I* and $I_2$(B); the solid line is the recommended calibration curve given by eq 10a of the text.

In Table 2, we give the simulated mean value of R** (in parentheses) as well as those predicted from the calibration curve of eq 10. The differences between the two determinations of ~0.03 Å, should be regarded as inherent errors of the method. Finally, to translate the length of this spring-gauge, $R^{**}$, to a cavity diameter, the van der Waals radius of the I* atoms should be added:

$$D = R^{**} + 2R_{vdW} \quad \text{where} \quad R_{vdW} = 2.18 \text{ Å} \qquad (11)$$

The hyperbolic nature of the curve makes it clear that at large separations, $R^{**} > 7$ Å, small measurement errors in the spectrum can lead to a large uncertainty in the determination of the internuclear separation. In cavity sizing applications, an accuracy of ~0.1 Å can be expected in the range $8 < D < 12$ Å.

To test the utility of the calibration curve in heterogeneous media, we consider the solid solutions of Kr/Xe. A very large sampling of configurations would be necessary for the realistic simulation of a solution of a given composition. Instead, for a given realized configuration of a given stoichiometry, we simply use the obtained values of emission peak versus internuclear distance to test the validity of eq 10. The simulated points nicely fit the proposed function as illustrated in the plot of Figure 6 (open circles). This agreement most directly illustrates the insensitivity of the spectral shift to the nature of the host, what was empirically described above as an ideal mixing property. It should now be obvious that the linear dependence of the spectral shift in wavelength on mixing fraction is the result of the nearly linear dependence of the cavity size on mixing and the hyperbolic dependence of the difference in potential energy on cavity size (Figure 6).

Finally, as a direct implementation of the proposed application, we use eq 10 to obtain $R^{**}$ values from previously reported spectral shifts in liquids. As in the case of the solids, the obtained $R^{**}$ values very closely follow the internuclear separation of the solvent molecules (see Table 2). The only outlier in this comparison is $CS_2$, in which the I*−I* separation seems to be nearly 2 Å larger than that of the solvent. There is a significant discrepancy between the present values of $R^{**}$ and those reported earlier.[2] This discrepancy can be traced to the approximations made in the prior work. The most significant error arises from the use of the approximate Morse form for $I_2(B)$ as opposed to the RKR potential used here. Moreover, the reproduction of the spectra in the present treatment is achieved by treating the problem in its full dimensionality, as opposed to the 1-D analysis (configuration coordinate) given in the prior treatment. Here, the entire solid state data set is reproduced with the two coefficients of the I*−I* exponential potential as the only adjustable parameters. We may therefore conclude that this potential is well-determined by the present analysis.

## Conclusions

The near-IR emission of $I_2$, which can be induced by a variety of photoexcitation schemes, provides a simple and sensitive means for determining the size of the cavity in which the molecule resides. Although the spectral widths of these transitions are broad, a rather accurate determination of cavity sizes, to within ±0.1 Å, is possible in the range $8 < D < 12$ Å. The spectral widths can be used to obtain information about cavity size distributions, following our treatment of line profiles in mixed hosts. More specific to the case of $I_2$ in mixed Kr/Xe matrixes, it is clear that the samples are homogeneous solutions. As such, these systems can be used to understand effects of local cage asymmetry on dynamics and in particular on the effect of electronic caging which arises from the cancellation of off-diagonal electronic matrix elements by the local symmetry of perturbers.[11] Finally, the parametrization of the I*I* potential to reproduce the observed line shape in neat matrixes is quite valuable, as this provides effective solvated potentials that enable the understanding of both time and frequency domain spectroscopy in this important model system.

**Acknowledgment.** This research was funded under a grant from the US AFOSR (F49620-01-1-0449).

## References and Notes

(1) Mulliken, R. S. *J. Chem. Phys.* **1971**, *55*, 288.
(2) Benderskii, A. V.; Zadoyan, R.; Apkarian, V. A. *J. Chem. Phys.* **1997**, *107*, 8437.
(3) Kubo, W.; Murakoshi, K.; Kitamura, T.; Yoshida, S.; Haruki, M.; Hanabusa, K.; Shirai, H.; Wada, Y.; Yanagida, S. *J. Phys. Chem. B* **2001**, *105*, 12809.
(4) John, R. K.; Kumar, D. S. *J. Appl. Polym. Sci*. **2002**, *83*, 1856.
(5) Zhong, J. C.; Misaki, Y.; Munakata, M.; Kuroda-Sowa, T.; Maekawa, M.; Suenaga, Y.; Konaka, H. *Inorg. Chem.* **2001**, *40*, 7096.
(6) Bhatia, S. K.; Liu, F.; Arvind, G. *Langmuir* **2000**, *16*, 4001.
(7) Nakashima, S.; Norimoto, M.; Harima, H.; Hamanaka, Y.; Grigoryan, L. S.; Tokumoto, M. *Chem. Phys. Lett.* **1997**, *268*, 359.
(8) Flachenecker, G.; Behrens, P.; Knopp, G.; Schmitt, M.; Siebert, T.; Vierheilig, A.; Wirnsberger, G.; Materny, A. *J. Phys. Chem. A* **1999**, *103*, 3854.
(9) Demontis, P.; Suffritti, G. B.; Tilocca, A. *J. Phys. Chem. B* **1999**, *103*, 8141.
(10) Chachisvilis, M.; Garcia-Ochoa, I.; Douhal, A.; Zewail, A. H. *Chem. Phys. Lett.* **1998**, *293*, 153.
(11) Zadoyan, R.; Sterling, M.; Ovchinnikov, M.; Apkarian, V. A *J. Chem. Phys.* **1997**, *107*, 8446.
(12) Almy, J.; Kizer, K.; Zadoyan, R.; Apkarian, V. A. *J. Phys. Chem. A* **2000**, *104*, 3508.
(13) Helbing, I.; Chergui, M. J. *Luminescence*, **2001**, *94*, 611.
(14) Macler, M.; Heaven, M. *Chem. Phys.* **1991**, *151*, 219.
(15) Zadoyan, R.; Li, Z.; Ashjian, P.; Martens, C. C.; Apkarian, V. A. *Chem. Phys. Lett.* **1994**, *218*, 504.
(16) Bihary, Z.; Gerber, R. B.; Apkarian, V. A. *J. Chem. Phys.* **2001**, *115*, 2695.
(17) Bihary, Z.; Karavitis, M.; Gerber, R. B.; Apkarian, V. A. *J. Chem. Phys.* **2001**, *115*, 8006.
(18) Rowlinson, J. S.; Swinton, F. L. *Liquids and liquid mixtures*; Butterworth Scientific: London, 1982.
(19) Casavecchia, P.; He, G.; Sparks, R. K.; Lee, Y. T. *J. Chem. Phys.* **1982**, *77*, 1878.
(20) Lawrence, W. G.; Apkarian, V. A. *J. Chem. Phys.* **1994**, *101*, 1820.
(21) Yourshaw, I.; Zhao, Y.; Neumark, D. M. *J. Chem. Phys.* **1996**, *105*, 351.
(22) Lenzer, T.; Furlanetto, M. R.; Pivonka, N. L.; Neumark, D. M. *J. Chem. Phys.* **1999**, *110*, 6714.
(23) In the simulations of ref 20, a matrix and density dependent shift in the spin−orbit splitting Δ is deduced. A reexamination of the data shows that the observed dependencies of the spectral shifts can be reproduced by small adjustments to the pair potentials, without invoking a change in Δ.
(24) Barrow, F. B.; Yee, K. K. *J. Chem. Soc., Faraday Trans.* 2 **1973**, *69*, 684.
(25) Buchachenko, A. A.; Stepanov, N. F. *J. Chem. Phys.* **1996**, *104*, 9913. Buchachenko, A. A. *Chem. Phys. Lett.* **1998**, *292*, 273.
(26) Batista, V. S.; Coker, D. F. *J. Chem. Phys*. **1996**, *105*, 4033. Batista, V. S.; Coker, D. F. *J. Chem. Phys.* **1997**, *106*, 6923.
(27) Zadoyan, R.; Li, Z.; Martens, C. C.; Apkarian, V. A. *J. Chem. Phys.* **1994**, *101*, 6648.